

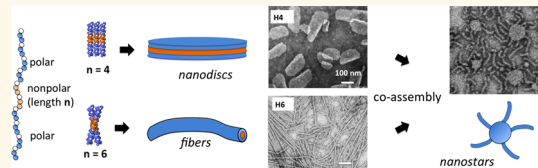


# Morphological Diversity and Polymorphism of Self-Assembling Collagen Peptides Controlled by Length of Hydrophobic Domains

Kenneth McGuinness, I. John Khan, and Vikas Nanda\*

Center for Advanced Biotechnology and Medicine, Robert Wood Johnson Medical School, Rutgers University, Piscataway, New Jersey 08854, United States

**ABSTRACT** Synthetic collagen mimetic peptides are used to probe the role of hydrophobic forces in mediating protein self-assembly. Higher order association is an integral property of natural collagens, which assemble into fibers and meshes that comprise the extracellular matrix of connective tissues. The unique triple-helix fold fully exposes two-thirds of positions in the protein to solvent, providing ample opportunities for engineering interaction sites. Inclusion of just a few hydrophobic groups in a minimal peptide promotes a rich variety of self-assembly behaviors, resulting in hundred-nanometer to micron size nanodisks and nanofibers. Morphology depends primarily on the length of hydrophobic domains. Peptide discs contain lipophilic domains capable of sequestering small hydrophobic dyes. Combining multiple peptide types result in composite structures of discs and fibers ranging from stars to plates-on-a-string. These systems provide valuable tools to shed insight into the fundamental principles underlying hydrophobicity-driven higher order protein association that will facilitate the design of self-assembling systems in biomaterials and nanomedical applications.



**KEYWORDS:** polymorphism · self-assembly · hydrophobicity · collagen mimetic peptides (CMPs)

**H**ydrophobic forces can be used to control protein self-assembly into nanoscale structures. There is considerable interest in engineering synthetic proteins that harness the structural and functional potential of supramolecular assemblies<sup>1–5</sup> for nanoscale engineering of biosensors, multistep catalysts, and smart stimulus-responsive materials. A detailed molecular-level understanding of the factors driving assembly is crucial to effectively engineer synthetic complexes. For example, knowing the rules for canonical Watson–Crick pairing of nucleotides has driven the exciting field of DNA origami, where synthetic oligonucleotides assemble into elaborate two- and three-dimensional forms.<sup>6,7</sup>

Protein complex interfaces often incorporate clusters of hydrophobic amino acids, serving as sticky surfaces for adhesion.<sup>8–11</sup> Surface hydrophobicity is tightly regulated in natural proteins,<sup>12,13</sup> and inappropriate presentation of residues on the surface can lead to aggregation and pathogenesis. In sickle cell anemia, a single hydrophilic to hydrophobic amino acid substitution on the

surface of hemoglobin results in massive protein aggregates that distort red blood cells.<sup>14</sup> Hydrophobic stretches in protein sequences can contribute to amyloidogenesis.<sup>15–20</sup>

Hydrophobicity plays an important role in protein engineering, optimizing core interactions is a critical step in *de novo* design.<sup>21–26</sup> Adjusting surface hydrophobicity can be used to enhance protein solubility.<sup>26,27</sup> The extensive use of hydrophobicity in self-assembling block copolypeptides,<sup>28,29</sup> peptide amphiphiles,<sup>30–33</sup> small peptides,<sup>34–37</sup> and foldamers<sup>38,39</sup> demonstrates the tremendous utility of this force in the broader field of nanostructural molecular engineering.

Limited structural information on multi-protein complexes makes it challenging to determine how interface size, geometry, charge, hydrophobicity, and other factors may contribute to the strength and specificity of interactions. As a complement to the study of natural proteins, synthetic peptides have the potential to be a powerful system for exploring hydrophobicity-driven assembly.

\* Address correspondence to  
nanda@cabm.rutgers.edu.  
Phone: 732-235-5328.

Received for review September 22, 2014  
and accepted November 12, 2014.

Published online November 12, 2014  
10.1021/nn505369d

© 2014 American Chemical Society

**TABLE 1. Model Peptide Sequences**

	sequence	morphology
H2	(POG) <sub>3</sub> POGPOLIG(POG) <sub>4</sub>	disc
H3	(POG) <sub>3</sub> POGP <del>I</del> GLIG(POG) <sub>4</sub>	disc
H4	(POG) <sub>3</sub> POGLIGLIG(POG) <sub>4</sub>	disc
QH4	(POG) <sub>3</sub> QQGLIGLIG(POG) <sub>4</sub>	disc
H5	(POG) <sub>3</sub> PIGLIGLIG(POG) <sub>4</sub>	disc + fiber
H6	(POG) <sub>3</sub> LIGLIGLIG(POG) <sub>4</sub>	fiber

The triple-helix fold of collagen is an attractive molecular scaffold for studying protein–protein interactions and higher order assembly. Unlike nearly all other protein folds, which assemble around a hydrophobic core, the three strands of the triple-helix associate through a network of backbone–backbone interchain hydrogen bonds. As a result, hydrophobic groups on the surface are not expected to interfere with core folding, as seen in off-pathway intermediates of globular proteins.<sup>40–43</sup> The collagen triple helix is formed by tandem repeats of X–Y–Gly triplets, where X and Y residues are solvent exposed and where glycine is critical for core assembly.<sup>44</sup> In natural collagens, hydrophobic residues at the X and Y positions are significantly under-represented relative to globular proteins (approximately 8% of residues in type I collagen, Table S1 (Supporting Information), compared to 40% for myoglobin, a typical globular fold). Those that are present occur in periodic clusters every 231–237 residues, promoting assembly of triple-helices into higher order fibers with a characteristic 67 nm spacing.<sup>45–47</sup> As with other proteins, hydrophobicity of collagen appears to be tightly regulated, playing an important role in the process of self-assembly.

Collagen mimetic peptides (CMP) have been used to study self-assembly with a number of molecular strategies ranging from electrostatic interactions to metal coordination.<sup>30,48–59</sup> Despite their short length (~20–40 amino acids), CMPs effectively recapitulate many features of their much larger (over 1000 amino acids long) natural counterparts. We specifically probe the effect hydrophobicity plays in collagen assembly by designing CMPs incorporating contiguous blocks of hydrophobic residues at nonglycine positions (Table 1). Self-assembly of CMPs into fibers or plates is observed, where subtle changes in the hydrophobic residue pattern lead to dramatic switches in nanoscale morphology.

**Simulations of CMP Self-Assembly.** We expected that both the pattern and extent of hydrophobicity along the triple helix would be important parameters in directing self-assembly. Given 10 amino acid triplets (X–Y–Gly) per 30-residue peptide, there are nominally  $2^{10} = 1024$  possible combinations of hydrophobic and hydrophilic triplets. To rapidly identify those sequences capable of forming unique nanostructures, we implemented a coarse-grained model of self-assembly,

simulating the process of diffusion-limited aggregation (DLA).<sup>60,61</sup> More sophisticated simulation approaches of hydrophobic peptide self-assembly have been developed that include internal degrees of freedom within and between polypeptide chains,<sup>62,63</sup> but we chose rigid body docking of rods as the CMPs studied here are within an order of magnitude shorter than the persistence length of collagen.<sup>64</sup> In DLA, higher-order structures emerge through the stepwise accretion of monomers onto a growing assembly (Figure S1B,C, Supporting Information); this model assumes that monomer concentrations are sufficiently low that diffusion is the limiting factor in assembly kinetics. This method was attractive as it had been shown to replicate experimentally observed morphologies for systems of self-assembling peptides<sup>65,66</sup> and structural proteins elastin<sup>67</sup> and collagen.<sup>68</sup> Although we did not know *a priori* whether assembly of CMP peptides would proceed in a diffusion-limited or activated manner, such DLA-based simulations were able to explain experimentally observed features of assembled collagen fibers.<sup>69,70</sup>

## RESULTS AND DISCUSSION

We adapted a DLA simulation protocol from previous collagen studies.<sup>68</sup> The triple-helix was treated as a rigid rod composed of 10 spheres, with each sphere representing a hydrophobic (*h*) or polar (*p*) X–Y–Gly triplet positioned along the triple-helix surface. The source code used for these simulations is available in the Supporting Information. From the 1024 pattern combinations, we chose to focus on *pppphhffff*, where *p* ≡ Pro-Hyp-Gly (POG) and *h* ≡ Leu-Ile-Gly (LIG) (Figure 1A). The choice of hydrophobic residues was based on the high independent frequencies of Leu and Ile at X and Y positions respectively of natural fibrillar collagens.<sup>71</sup> Leucine has also been shown to promote higher order assembly in other CMP designs.<sup>59,72</sup> Simulations predicted this pattern would form dislike structures (Figure 1B).

**CMP H4 Assembles into Nanodiscs.** Transmission electron microscopy (TEM) images of H4 were consistent with the DLA prediction of a dislike morphology. Specifically, three features of the DLA models were observed by TEM (Figure 1c): (1) H4 discs were frequently observed to extend end-on from the hydrophobic carbon coated copper EM grid, consistent with a hydrophobic disc edge adhering to the surface; (2) thickness of these discs was estimated to be ~10 nm, equivalent to the length of one peptide, which would be expected if the peptides were assembling perpendicular to the plane of the disc; (3) rosette structures were observed in multiple preparations of H4, consistent with fractal dendritic DLA-type aggregation in two dimensions.<sup>65</sup> The lack of sharper, well-defined dendritic structures may have been due to fluidity of the disc phase, allowing internal rearrangements to

minimize the surface energy of the aggregate. An alternate process for rosette formation would be the association of fully assembled discs, rather than

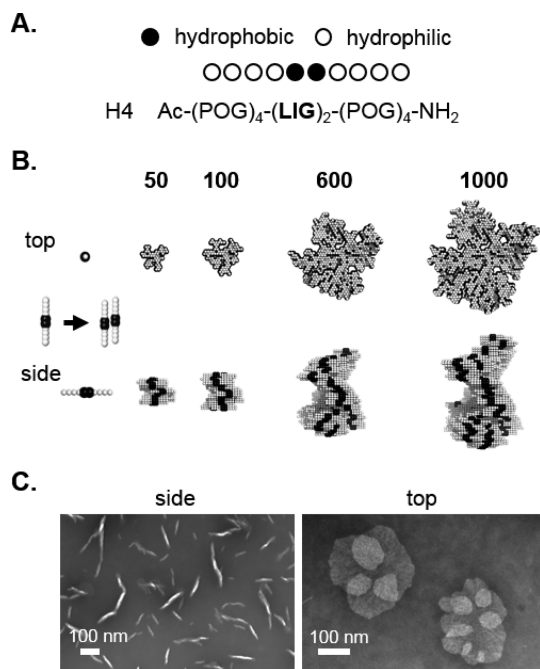


**Figure 1.** (A) Coarse-grained model of the H4 sequence. Each rod consists of 10 spheres, each sphere representing a triplet of amino acids. (B) DLA simulation trajectory of 1000 pppphhffff rod-generated platelike structures. Discs pictured correspond to small assemblies approximately 50 nm in diameter. (C) Electron micrographs of H4.

accretion of monomers through DLA. We were not able to discriminate between these two mechanisms based on the existing observations.

Although rosettes were consistently found, the dominant H4 morphology was a rounded disc. H4 disc diameters ranged from 50 nm to 1  $\mu$ m. In many cases, the plates appeared to be flexible, depositing on the grid in shapes resembling curved “potato chips” (Figure 2 and Figure S3, Supporting Information), indicating these structures lacked the crystallinity and rigidity found in other designed CMP plates.<sup>48,49,73</sup>

Using circular dichroism (CD) spectroscopy, we confirmed that the H4 peptide assembled into a triple-helix with a cooperative unfolding transition at 33 °C (Figure 3A,B). Observed *d*-spacings from wide-angle X-ray scattering (WAXS) of supersaturated H4 solutions further supported the presence of triple-helices in the aggregate phase. Bragg diffraction peaks at 11.7 and 12.7 Å (Figure 3C) were consistent with previous reports for the lateral packing of collagen triple-helices.<sup>73,74</sup>

The thickness of H4 nanodiscs that deposited end-on ascertained by TEM matched the length of triple helix. This was confirmed by atomic force microscopy (AFM) (Figure 4A). Analysis of many fields revealed height dimensions that occurred in multiples of 7–8 nm (Figure 4B,C), close to the expected length of a CMP of 8.6 nm (30 residues  $\times$  0.286 nm rise/residue). Over multiple experiments, a wide range of

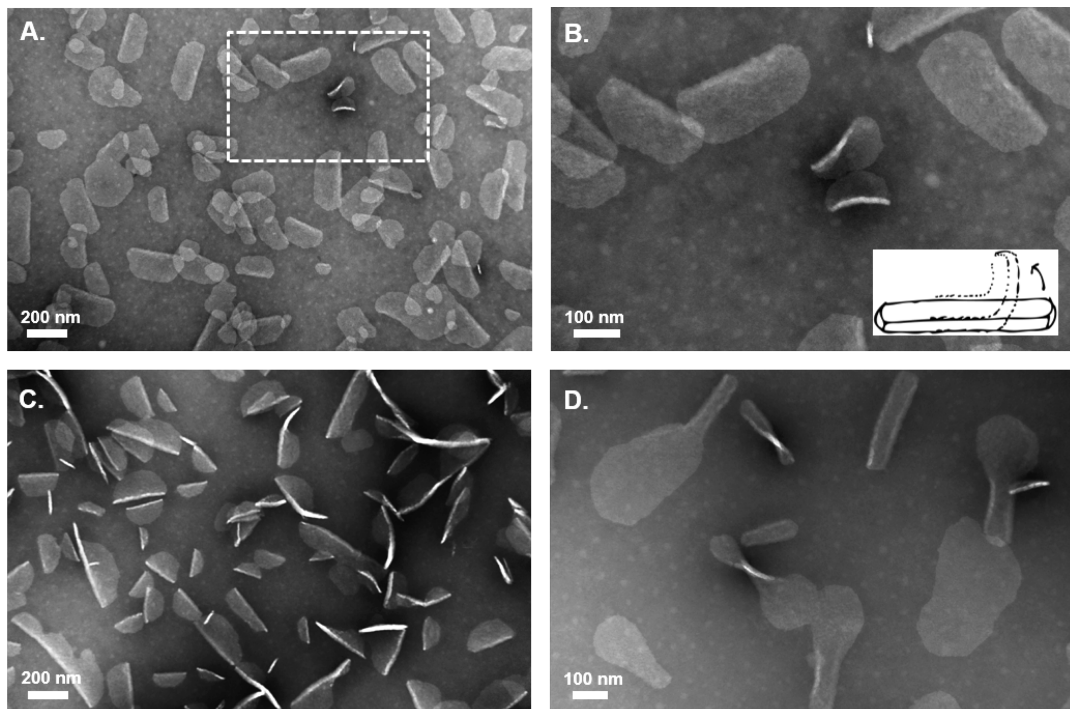


**Figure 2.** Transmission electron microscopy of H4 morphology. (A) This field shows numerous discs alone or overlapping adjacent disks. (B) Close-up of two H4 discs in field A curving as shown in the drawing. (C) Multiple curved discs and discs perpendicularly aligned to the electron beam. (D) Another field highlighting disc flexibility.

heights from 6–500 nm were observed for H4 (Figure S5, Supporting Information), all maintaining an overall dislike morphology, suggesting that significant stacking of discs could occur.

A reduction in sequence hydrophobicity was predicted to maintain a dislike morph due to limited registry interactions between triple-helices that would

minimize surface exposed hydrophobic residues. Replacing one leucine in H4 with proline produced H3 (Table 1), which folded into a triple-helix,  $T_m$  of 41 °C (Figures S4 and S6, Supporting Information), and self-assembled into plates (Figure S9A, Supporting Information). Similarly, H2 formed a triple-helix with a  $T_m$  of 50 °C (Figures S4 and S6, Supporting Information) and was shown by TEM to form plates similar to H4 (Figure S9B, Supporting Information).

**CMP H6 Forms Nanofibers.** Increasing the hydrophobicity of a collagen sequence by adding an additional hydrophobic triplet (*ppphhhpppp*) was also predicted in DLA simulations to produce dislike structures with variable thickness due to staggered interactions between adjacent monomer rods (Figures S1C and S3, Supporting Information). Surprisingly, the CMP equivalent of this pattern, H6, formed uniform fibers, strikingly different from the model. Fibers observed by TEM varied from ~50 nm to several microns in length and 6–11 nm in width (Figure 5A and Figure S3C1, Supporting Information). Occasional evidence of branching and punctate structures was observed, possibly indicating prefibril intermediates or small discs (Figure S3D, Supporting Information). Upon heating and reannealing, H6 fibers formed straight, aligned clusters several microns in length (Figure 5B and Figure S3C2, Supporting Information).

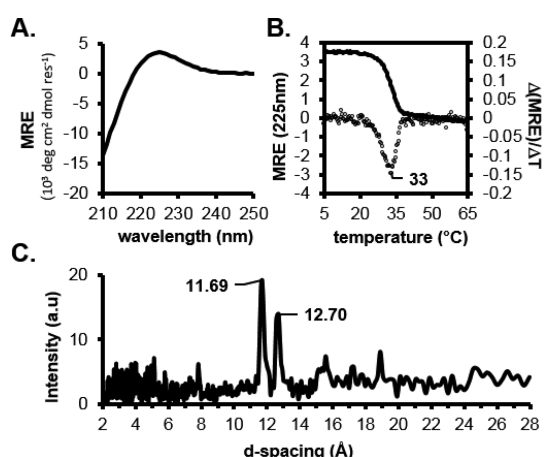


Figure 3. H4 forms triple-helices. (A) CD spectrum shows positive MRE (mean residue ellipticity) band at 225 nm, consistent with triple-helical structure. (B) Thermal denaturation profile shows cooperative unfolding of H4 with a  $T_m$  of 33 °C. (C) WAXS of H4 shows interhelical  $d$ -spacing consistent with fiber packing observed in natural collagens.

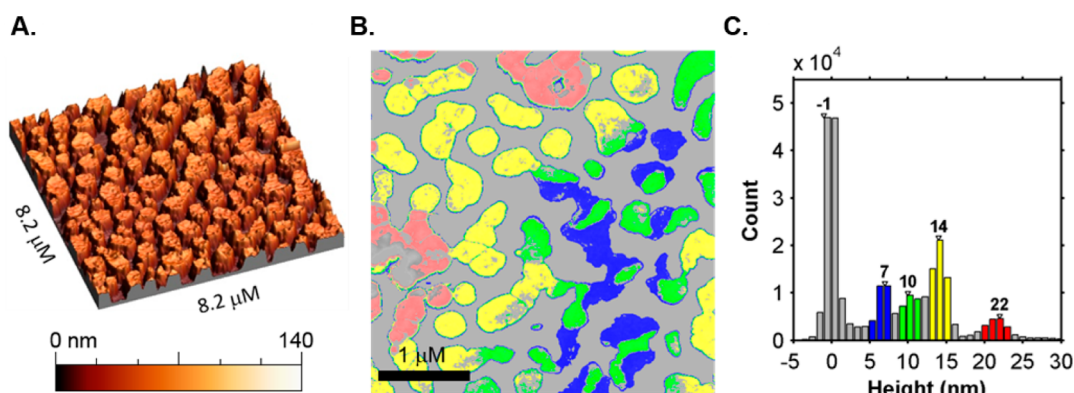


Figure 4. AFM of H4 discs: (A) 3D representation of discs, (B) coloring of AFM field based on height, (C) histogram of H4 heights observed in (B).

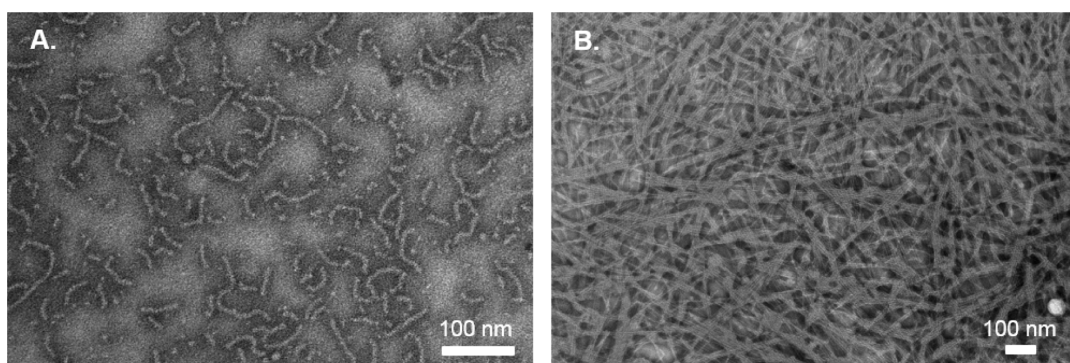
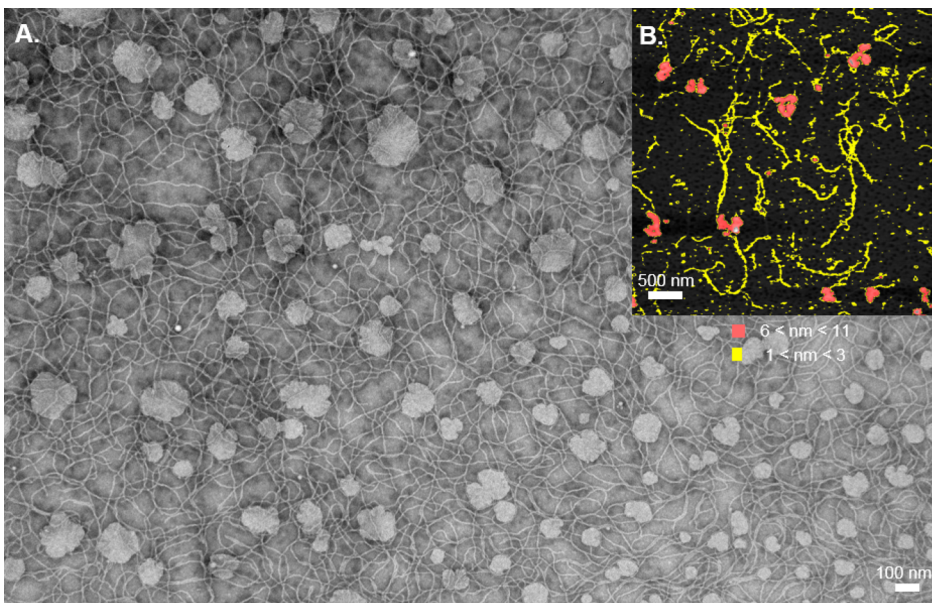


Figure 5. Characterization of H6 (A) incubated at 4 °C (B) heated to 30 °C and annealed at 4 °C.



**Figure 6. Characterization of H5 (A) TEM and (B) AFM where yellow signifies 1–3 nm height features and red signifies 6–11 nm height features.**

One potential explanation for the unexpected fiber morphology was the misfolding or unfolding of H6 leading to different modes of aggregation. Although H6 clearly formed triple-helices as measured by CD, the peptides were marginally stable with a  $T_m \sim 15$  °C (Figures S4 and S6, Supporting Information). On the basis of its physiochemical properties, the (LIG)<sub>3</sub> hydrophobic domain of H6 has a high computed propensity to form amyloids,<sup>75</sup> and previous examples of cross- $\beta$  structures formed by amyloidogenic regions within CMPs have been described.<sup>17,76</sup> However, H6 fibers did not bind Congo Red, a common amyloid probe<sup>77</sup> (Figure S7A, Supporting Information), and no evidence of the twisted cross- $\beta$  structure was noticed in TEM images. H6 fibers were morphologically similar to those formed by other CMPs where triple-helical structure was required for higher order assembly.<sup>57</sup> If adjacent rods packed at an angle, then the resulting fiber would be a super helix of CMPs where fiber thickness matches the length of a peptide (Figure S11A, Supporting Information).<sup>78</sup> This type angular packing was not incorporated in the coarse-grained simulation, so this fiber morph would not be predicted.

**Morphology Is Determined by Hydrophobicity.** To determine whether the fiber morphology arises from the low structural stability of H6 or its increased hydrophobicity, we synthesized the peptide QH4 (Table 1) consisting of two hydrophobic triplets and one Gln-Gln-Gly. The polar amino acid glutamine is well tolerated at both the X and Y positions of the triple-helix, but does not confer the same stability as proline or hydroxyproline,<sup>71</sup> making it a suitable proxy for the low stability of H6 while maintaining the hydrophobicity of H4. QH4 folded into a triple-helix (Figure S4, Supporting Information) and despite a 9 °C lower  $T_m$  than H4

(Figure S6, Supporting Information), the peptides formed plates (Figure S8, Supporting Information), thus supporting a model where length of hydrophobic region is the primary determinant of assembly morphology.

**Polymorphic Behavior of H5.** The collective properties of existing CMPs pointed to a morphological bifurcation point related to hydrophobicity between H4 and H6. Below this point, the disc morph dominated, with only minor populations of fibers seen in H2, H3, and H4 TEM fields (Figures S2 and S9, Supporting Information). Above this point, fibers were predominantly formed. To further pinpoint where this transition occurred, we examined H5 (Table 1). H5 folded into a triple-helix with the stability of 24 °C (Figures S4 and 6, Supporting Information). Consistent with it sitting on a saddle point between two morphologies, H5 was observed by TEM to assemble into major populations of *both* fibers and plates (Figure 6A and Figure S10, Supporting Information). Fiber widths and lengths were calculated to be 7.5–9.5 nm and several microns, respectively. H5 disc diameters were 50–200 nm. AFM confirmed the presence of fibers and plate morphs with fiber heights between 1 and 3 nm and plates with heights 6–11 nm (Figure 6B). Similarly to H6, H5 did not bind Congo Red (Figure S7B, Supporting Information).

**H4 Discs Sequester Hydrophobic Dyes.** Self-assembling amphiphilic peptides and peptidomimetics can produce lipophilic domains capable of sequestering small molecules and acting as vehicles for drug delivery.<sup>79–81</sup> The H4 nanodiscs are similarly able to bind solvatochromatic dyes such as Sypro Orange (SO), which has an enhanced quantum yield when bound to hydrophobic surfaces. Confocal microscope images of H4 + SO show effective nanodisc sequestration of the dye (Figure 7A).

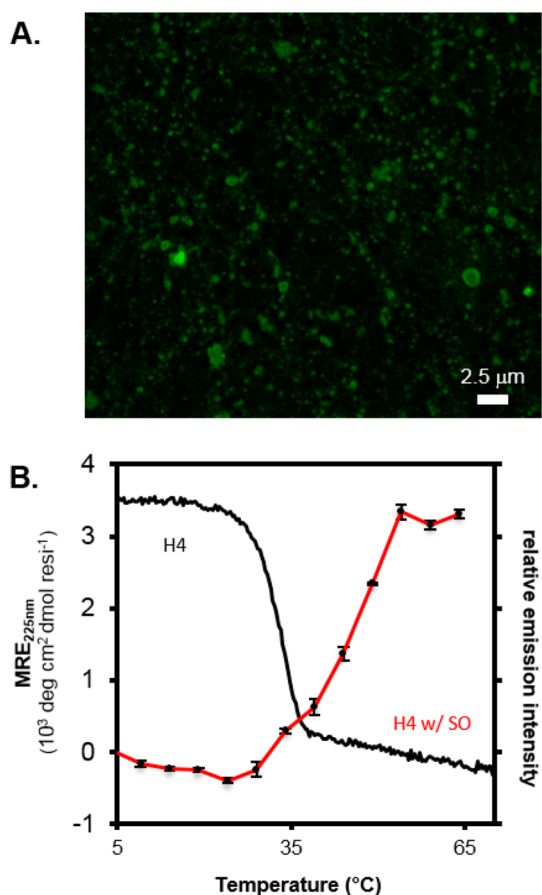


**Figure 7.** (A) Confocal fluorescence microscopy of SO-H4 solution. (B) Differential scanning fluorimetry of H4 with Sypro Orange (red) and circular dichroism thermal denaturation melt of H4 (black).

SO intensity increases when discs are heated above the  $T_m$  of H4 (Figure 7B), which is typically observed for globular proteins upon unfolding.<sup>82</sup> This suggests that denaturation of the H4 discs exposes greater hydrophobic surface area for SO binding.

#### Multicomponent Peptide Nanostars and Plates-on-Strings.

Natural collagen proteins make use of hydrophobic interactions to bind other proteins such as integrin receptors.<sup>83</sup> Likewise, we would expect the hydrophobic CMPs to interact with other molecules that also present exposed hydrophobic surfaces. We explore two cases of multicomponent interactions, H4/H6 nanostars and H4/amyloid peptide tandem plate assemblies.

As postulated earlier, one possible structural model for the fiber morph is that of a helical tape<sup>78</sup> formed by CMP rods that pack at an angle. A model of what such a structure might look like (Figure 8A and Figure S11A, Supporting Information) suggests a fiber with highly exposed hydrophobic ends. AFM of H6 reveals an undulating height profile varying from 1.5 to 6 nm, consistent with a helical tape (Figure S12, Supporting Information). Assuming H4 discs have hydrophobic edges and H6 fibers have hydrophobic ends, combining the two would be expected to generate conjoined nanostar-like structures with fibers alighting from the edges of discs (Figure 8A and Figure S11B, Supporting Information). Consistent with this, EM images of H6:H4 mixtures revealed fibers branching from discs (Figure 8B and Figure S11C, Supporting Information). We note similar behavior in some H5 TEM fields where fibers are seen originating from the edges of discs.

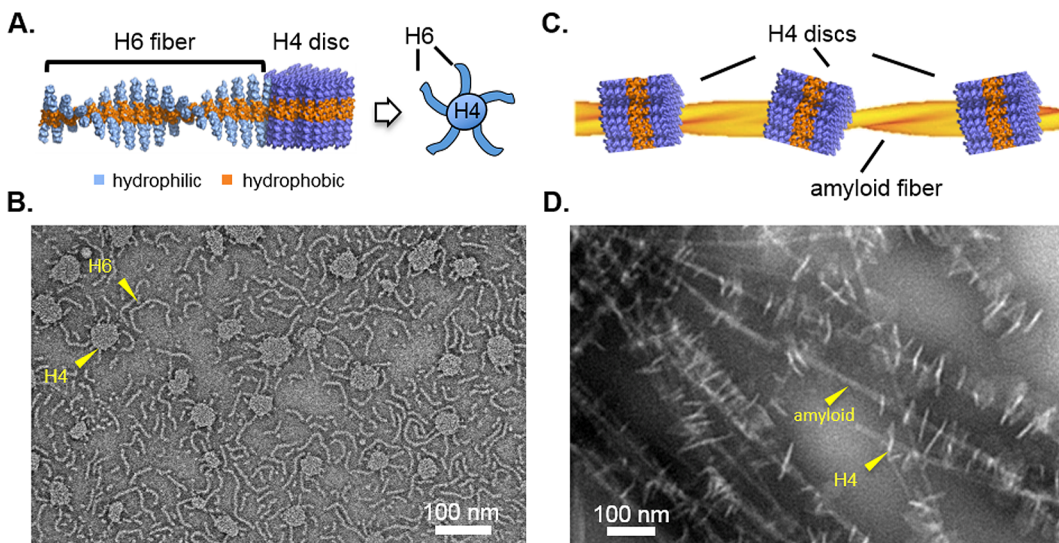


**Figure 8.** (A) Hydrophobic interactions between H6 fiber and H4 disc models suggest formation of nanostar structures when mixed. (B) TEM of a 2:1 ratio of H6:H4 peptides confirms fibers matching H6 morphology attached to the disc edges. (C) The NdQ peptide forms an extended hydrophobic amyloid fiber that should interact with the hydrophobic edges of H4 discs. (D) TEM of a 1:1 ratio of H4 discs mixed with amyloid fibers shows tandem discs aligned perpendicular to both the grid surface and the long axis of the amyloid fibril, consistent with the proposed interaction model.

The observation that H6 fibers only interact at their ends suggests the packing geometry of the fiber shields the central hydrophobic residues. If an alternative type of fiber were to present a hydrophobic surface, then discs might be expected to attach along the fiber length rather than only at the ends (Figure 8C). Using a short hydrophobic amyloidogenic peptide, NdQ, we were able to generate extended beta-helical structures that would presumably present hydrophobic side chains along the full length of the fiber (Figure S13, Supporting Information). When these were combined with H4, multiple tandem discs attached perpendicularly to the fibers (Figure 8D). In several instances, discs would bundle individual fibers together, aligning them over micron distances.

## CONCLUSIONS

Collagen is on the cusp of solubility, which is functionally advantageous given its role in higher order assembly processes in biology. Small changes in sequence hydrophobicity induce rapid assembly and large changes in morphology. This sequence-dependent sensitivity of CMP assembly has been observed many times before: increasing core POG repeat length of metalligated CMP assemblies results in shifts from meshes to florettes to saddle-like structures<sup>53</sup> and increasing the number of core bipyridines lead to the formation of fibers,<sup>55</sup> discs<sup>54,56</sup> and then to hollow spheres.<sup>56</sup> Electrostatically driven assembly of CMPs containing acidic and basic regions show similar sequence sensitive polymorphism, where arginine and glutamic acid formed D-periodic fibers,<sup>50</sup> whereas lysine and aspartic acid formed hydrogels.<sup>51</sup> This is a general property expected of self-assembling system where the sum of small forces in local molecular interactions exerts significant influence on the properties at the aggregate level.

Certain features of the H-series CMPs could serve as starting points for developing functional materials. Given the observation that single amino acid changes can drive dramatic variations in the self-assembly phenotype, it should be possible to design switchable peptides that interconvert between two nanoscale morphologies on the basis of environmental perturbations leading to potential biosensor or controlled-release applications.

Additionally, the ability to control the structure at the scale of microns and above is important for engineering materials that interact with cells.<sup>84,85</sup> H4 and H6 CMPs form structures on this length scale and could be further developed to provide cell-scale interactions. The ability of these peptides to interact with other proteins suggests a modular design strategy where structure and function are separated into different molecules. A structural matrix scaffold that forms micron scale fibers such as the amyloids or natural collagens could be decorated with peptides that provide chemical or biological functionality.

In the early evolution of natural collagen, such a propensity for polymorphism might have been advantageous, allowing smaller molecules to rapidly explore and optimize the assembly of functionally useful nanoscale forms. In extant collagens which are generally much larger, hydrophobicity is tightly constrained, with only two triplets in type I collagen out of 300 having a tandem pair of hydrophobic amino acids at X and Y positions akin to the H2 peptide. Longer hydrophobic stretches such as those incorporated into H3–H6 are extremely rare, with H4-like LIGLIG sequences in types V and XI collagens. How such hydrophobic sites function in the context of natural collagen versus model peptides will be an interesting area of future study.

Higher resolution structural information will be critical in order to fully understand how hydrophobicity drives nanoscale morphology. A change in the packing angle between adjacent triple helices would explain the difference between the fiber and disc morphs. However, the relative amounts of these two species going from H2 to H6 could depend both on energetic and kinetic factors in assembly.

Even within the scope of simple *h/p* CMP designs, this work has only just scratched the surface of the sequence diversity available. In addition to length of the hydrophobic core, further designs incorporating different patterns of hydrophobic/hydrophilic residues can be designed to potentially produce a rich library of higher order structures. Further cycles of simulation, design, and experimental characterization will likely improve the accuracy of predictive tools and enhance our understanding of hydrophobic forces in protein self-assembly.

## MATERIALS AND METHODS

**Diffusion Limited Aggregation (DLA).** The DLA simulations were conducted in a 3D hexagonal lattice (Figure S1A, Supporting Information). The seed for each DLA simulation was a discretized rigid rod composed of 10 spheres. Each sphere represented an XYG triplet of amino acids and was either hydrophobic (*h*) or polar (*p*). A seed rod was placed at the center of the simulation, and additional rods were released and allowed to move randomly until either they contacted the aggregate or they moved too far away from the aggregate and were discarded (Figure S1A, Supporting Information). Simulations of each of the 1024 possible

sequence combinations were repeated 100 times to assess convergence of nanoscale morphs. A suitable interaction state was defined as greater than two hydrophobic groups in contact. Representative assembly structures were chosen for presentation. The peptide H4 was modeled after the DLA rod *ppphhhffff*. The peptide H6 was modeled after *ppphhhffff*. JAVA source code for the simulations are in supplementary file collagenDLA.zip (Supporting Information).

**Peptide Synthesis and Purification.** Peptides were synthesized using solid-phase Fmoc chemistry, purified by reversed-phase HPLC, and verified using mass spectrometry at the Tufts

University Core Facility (<http://tucf.org>) (Figure S14–20, Supporting Information). H6, H5, H4, and H3 were purified to >95% purity by reversed-phase HPLC. Due to issues with synthesis, H2 purity was low, ~80%. N- and C- termini were acetylated and amidated, respectively. Peptides were dialyzed in filtered deionized water, lyophilized and kept in –20 °C. Peptides were weighed and resuspended in 10 mM phosphate buffer, pH 7.4. Collagen peptide concentrations were confirmed by measuring the absorbance at 214 nm, using an extinction coefficient of 2200 M<sup>-1</sup> cm<sup>-1</sup> per peptide bond on an AVIV model 14DS UV-vis spectrophotometer. Peptide NdQ, sequence NYFYSLFdQG (dQ = D-glutamine) was purified to >95% and solvated in 50 mM Tris pH 8.0 buffer with 30 mM NaCl, 2.5% glycerol, and 10 mM DTT.

**Circular Dichroism (CD).** CD experiments were performed on an Aviv model 400 spectrophotometer. Optically matched 1 mm path length quartz cuvettes (Model 110-OS, Hellman USA) were used. Peptide solutions were prepared and kept at 4 °C for a minimum of 48 h prior to measurement. Before measurement, peptide concentrations were diluted to 0.20 mM to reduce excess absorption at lower wavelengths. Wavelength scans were taken from 260 to 200 nm at 4 °C. Thermal denaturation melts were monitored at 225 nm with a temperature step of 0.3 °C and a 2 min equilibration period from 4–80 °C. Savitzky–Golay smoothing of the first derivative of the denaturation profiles was carried out over a span of 11 points using a third-order polynomial.<sup>86</sup> The melting temperature ( $T_m$ ) of each melt was assigned to the extrema of the first derivative of the denaturation profiles.

**Congo Red Assay.** A stock 5 μM Congo Red (CR) (C6767, Sigma-Aldrich) solution was prepared using deionized water. Concentration of CR was measured using the absorption value at 505 nm and the extinction coefficient of 59300 M<sup>-1</sup> cm<sup>-1</sup>.<sup>77</sup> A volume of 12 μL of 3 mM peptide solution was mixed with 280 μL of stock CR solution. Wavelength measurements of peptide solutions with and without CR, CR alone, and buffer were taken from 400–600 nm.

**Transmission Electron Microscope (TEM).** Collagen peptide samples were prepared at concentrations ranging from 2 to 10 mM and incubated at 4 °C for 2 weeks prior to imaging. NdQ was prepared at concentrations of 0.5 mM, and fibers were observed within 3 h. H6 and H4 samples were combined 1:1, 1:2, and 2:1 wt/wt ratios with a total weight of 3.6 mg and dissolved in pH 7.4 phosphate buffer. NdQ and H4 samples were combined at a 1:1 molar ratio. A volume of 5 μL of peptide solution was deposited on a copper grid coated with carbon (Electron Microscopy Sciences CF-400-Cu). After standing for two minutes to ensure deposition, excess buffer was wicked away using filter paper. The grid was then negatively stained with 1% phosphotungstic acid (PTA) pH 7.0 for 2 min, and excess stain was wicked away. Afterward, the grids were left to dry for at least 2 min in ambient conditions before imaging. Images were captured using a Philip 420 Electron Microscope at 80 kV.

**Atomic Force Microscopy (AFM).** For H4 and H6 solutions the method of Xu *et al.* was followed.<sup>73</sup> Briefly, silicon wafers were cleaned with a series of alcohols and subjected to sonication and incubation. The silicon wafers were then dried with nitrogen, placed on a glass slide with adhesive, and cooled before sample deposition. Excess sample was then removed using deionized water and dried for 20 min at room temperature. Three scans were taken for each measurement using an Agilent 5500 in tapping mode in air, with a Multi75a probe (Bruker MPP-21120-10).

H5 solutions were visualized using a MFP-3D-Bio AFM with a Nikon microscope (Asylum Research, Santa Barbara, CA). Measurements were made using contact mode in air with a SNL-10 probe (Bruker) on samples that were prepared on freshly cleaved mica. Samples were rinsed with deionized water and dried with argon prior to imaging. Data was analyzed using a combination of Gwyddion,<sup>87</sup> WSXM,<sup>88</sup> and MATLAB<sup>89</sup> software packages.

**Wide-Angle X-ray Scattering (WAXS).** Supersaturated solutions of H4 were prepared by placing peptide powder in a glass capillary (special glass 1 mm o.d.; Charles Supper Company, Natick, MA), and then solvent was added on top of the powder. The solvent was allowed to soak the powder for at least 2 weeks at 4 °C to ensure sufficient hydration.

The capillary was mounted in a Rigaku Geigerflex X-ray diffractometer with a sealed Cu target X-ray tube and Rigaku Osmic mirror focusing monochromator (Cu Kα;  $\lambda$  = 1.5418 Å). The nominal sample to detector distance was set at 2.2 cm. Data were collected by scanning along  $2\theta$  from 3° to 40° (step size 0.04°) with a 60 s count per step. The baseline of the data was subtracted using the software Jade Plus release 7.0.6 (Materials Data Inc., Livermore, CA).

**Differential Scanning Fluorimetry (DSF).** The method of Niesen *et al.*<sup>82</sup> was closely followed. A stock 50× solution of Sypro Orange (SO) (Sigma-Aldrich S5692-50 μL lot no. MKBP8121 V) was freshly made. The stock solution of SO was diluted with either H4 disc solutions or phosphate buffer to 5×. Samples were monitored using the  $\lambda_{ex}$  470 nm and  $\lambda_{em}$  610 nm wavelengths, with 2 and 6 nm slit-widths, respectively. H4 samples with SO were corrected for SO fluorescence. Three measurements were taken for each temperature step (4–64 °C in 5 °C increments at the same rate as the CD experiments), and an average and standard deviation was computed. Standard deviations were used as error bars. Experiments were performed using a Fluoromax-4 spectrophotofluorimeter (Jobin Yvon Horiba) with micro quartz cells (Starna Cell, Inc., cat. no. 3-3.30-Q-3).

**Confocal Fluorescence Microscopy.** H4 samples were prepared similarly to the DSF solutions. A 10–20 μL aliquot of the H4 solution was placed on microscope slides (Fisher cat. no. 12-544-7) and covered with glass coverslips (cat. no. 12-542-B, lot no. 101413-9). Slides were then incubated on ice for 20 min to ensure settling. The experiment was performed on a Leica TCS Sp8 G-STED microscope, and a red filter was used.

**Conflict of Interest:** The authors declare no competing financial interest.

**Supporting Information Available:** Supplemental figures, tables, and simulation source code are available in the supplement. This material is available free of charge via the Internet at <http://pubs.acs.org>.

**Acknowledgment.** National Institutes of Health Grant No. DP2 OD-006478 supported this research. K.M. was supported by a GAANN fellowship. We also thank Daniel Grisham for assistance with image processing and analysis, Patrick Nosker for the amyloid peptides, Michele Vittadello, Hiroshi Matsui, and Michael Kopka for access to AFM, data collection, and assistance with analysis, Smita Patel for access to fluorimetry, Jonathan Boyd from Leica-Microsystems for access to confocal microscopy, and Srinivas Annavarapu for helpful discussions.

## REFERENCES AND NOTES

- Fletcher, J. M.; Harniman, R. L.; Barnes, F. R.; Boyle, A. L.; Collins, A.; Mantell, J.; Sharp, T. H.; Antognazzi, M.; Booth, P. J.; Linden, N.; *et al.* Self-Assembling Cages from Coiled-Coil Peptide Modules. *Science* **2013**, *340*, 595–599.
- Ryadnov, M. G.; Bella, A.; Timson, S.; Woolfson, D. N. Modular Design of Peptide Fibrillar Nano- to Microstructures. *J. Am. Chem. Soc.* **2009**, *131*, 13240–13241.
- King, N. P.; Bale, J. B.; Sheffler, W.; McNamara, D. E.; Gonen, S.; Gonen, T.; Yeates, T. O.; Baker, D. Accurate Design of Co-Assembling Multi-Component Protein Nanomaterials. *Nature* **2014**, *510*, 103–108.
- King, N. P.; Sheffler, W.; Sawaya, M. R.; Vollmar, B. S.; Sumida, J. P.; Andre, I.; Gonen, T.; Yeates, T. O.; Baker, D. Computational Design of Self-Assembling Protein Nanomaterials with Atomic Level Accuracy. *Science* **2012**, *336*, 1171–1174.
- Gradisar, H.; Bozic, S.; Doles, T.; Vengust, D.; Hafner-Bratkovic, I.; Mertelj, A.; Webb, B.; Sali, A.; Klavzar, S.; Jerala, R. Design of a Single-Chain Polypeptide Tetrahedron Assembled from Coiled-Coil Segments. *Nat. Chem. Biol.* **2013**, *9*, 362–366.
- Rothenmund, P. W. Folding DNA to Create Nanoscale Shapes and Patterns. *Nature* **2006**, *440*, 297–302.
- Han, D.; Pal, S.; Nangreave, J.; Deng, Z.; Liu, Y.; Yan, H. DNA Origami with Complex Curvatures in Three-Dimensional Space. *Science* **2011**, *332*, 342–346.

8. Chothia, C.; Janin, J. Principles of Protein—Protein Recognition. *Nature* **1975**, *256*, 705–708.
9. Janin, J.; Miller, S.; Chothia, C. Surface, Subunit Interfaces and Interior of Oligomeric Proteins. *J. Mol. Biol.* **1988**, *204*, 155–164.
10. Miller, S.; Janin, J.; Lesk, A. M.; Chothia, C. Interior and Surface of Monomeric Proteins. *J. Mol. Biol.* **1987**, *196*, 641–656.
11. Jones, S.; Thornton, J. M. Prediction of Protein—Protein Interaction Sites Using Patch Analysis. *J. Mol. Biol.* **1997**, *272*, 133–143.
12. Miller, S.; Lesk, A. M.; Janin, J.; Chothia, C. The Accessible Surface Area and Stability of Oligomeric Proteins. *Nature* **1987**, *328*, 834–836.
13. Bowie, J. U.; Luthy, R.; Eisenberg, D. A Method to Identify Protein Sequences That Fold into a Known Three-Dimensional Structure. *Science* **1991**, *253*, 164–170.
14. Murayama, M. Molecular Mechanism of Red Cell “Sickling”. *Science* **1966**, *153*, 145–149.
15. Chiti, F.; Stefani, M.; Taddei, N.; Ramponi, G.; Dobson, C. M. Rationalization of the Effects of Mutations on Peptide and Protein Aggregation Rates. *Nature* **2003**, *424*, 805–808.
16. Pawar, A. P.; DuBay, K. F.; Zurdo, J.; Chiti, F.; Vendruscolo, M.; Dobson, C. M. Prediction of “Aggregation-Prone” and “Aggregation-Susceptible” Regions in Proteins Associated with Neurodegenerative Diseases. *J. Mol. Biol.* **2005**, *350*, 379–392.
17. Parmar, A. S.; Nunes, A. M.; Baum, J.; Brodsky, B. A Peptide Study of the Relationship between the Collagen Triple-Helix and Amyloid. *Biopolymers* **2012**, *97*, 795–806.
18. Wang, W.; Hecht, M. H. Rationally Designed Mutations Convert De Novo Amyloid-Like Fibrils into Monomeric Beta-Sheet Proteins. *Proc. Natl. Acad. Sci. U.S.A.* **2002**, *99*, 2760–2765.
19. Hilbich, C.; Kisterswoijke, B.; Reed, J.; Masters, C. L.; Beyreuther, K. Substitutions of Hydrophobic Amino-Acids Reduce the Amyloidogenicity of Alzheimers-Disease Beta-A4 Peptides. *J. Mol. Biol.* **1992**, *228*, 460–473.
20. Kim, W.; Hecht, M. H. Sequence Determinants of Enhanced Amyloidogenicity of Alzheimer’s Beta 42 Peptide Relative to a Beta 40. *J. Biol. Chem.* **2005**, *280*, 35069–35076.
21. Dahiyat, B. I.; Mayo, S. L. De Novo Protein Design: Fully Automated Sequence Selection. *Science* **1997**, *278*, 82–87.
22. Shifman, J. M.; Mayo, S. L. Modulating Calmodulin Binding Specificity through Computational Protein Design. *J. Mol. Biol.* **2002**, *323*, 417–423.
23. Degrado, W. F.; Lear, J. D. Induction of Peptide Conformation at Apolar Water Interfaces 1. A Study with Model Peptides of Defined Hydrophobic Periodicity. *J. Am. Chem. Soc.* **1985**, *107*, 7684–7689.
24. Ventura, S.; Vega, M. C.; Lacroix, E.; Angrand, I.; Spagnolo, L.; Serrano, L. Conformational Strain in the Hydrophobic Core and Its Implications for Protein Folding and Design. *Nat. Struct. Biol.* **2002**, *9*, 485–493.
25. Kamtekar, S.; Schiffer, J. M.; Xiong, H.; Babik, J. M.; Hecht, M. H. Protein Design by Binary Patterning of Polar and Nonpolar Amino Acids. *Science* **1993**, *262*, 1680–1685.
26. Jacak, R.; Leaver-Fay, A.; Kuhlman, B. Computational Protein Design with Explicit Consideration of Surface Hydrophobic Patches. *Proteins* **2012**, *80*, 825–838.
27. Trevino, S. R.; Scholtz, J. M.; Pace, C. N. Amino Acid Contribution to Protein Solubility: Asp, Glu, and Ser Contribute More Favorably Than the Other Hydrophilic Amino Acids in RNase SA. *J. Mol. Biol.* **2007**, *366*, 449–460.
28. Holowka, E. P.; Pochan, D. J.; Deming, T. J. Charged Polypeptide Vesicles with Controllable Diameter. *J. Am. Chem. Soc.* **2005**, *127*, 12423–12428.
29. Nowak, A. P.; Breedveld, V.; Pakstis, L.; Ozbas, B.; Pine, D. J.; Pochan, D.; Deming, T. J. Rapidly Recovering Hydrogel Scaffolds from Self-Assembling Diblock Copolymer Amphiphiles. *Nature* **2002**, *417*, 424–428.
30. Cui, H. G.; Webber, M. J.; Stupp, S. I. Self-Assembly of Peptide Amphiphiles: From Molecules to Nanostructures to Biomaterials. *Biopolymers* **2010**, *94*, 1–18.
31. Xu, H.; Wang, J.; Han, S.; Yu, D.; Zhang, H.; Xia, D.; Zhao, X.; Waigh, T. A.; Lu, J. R. Hydrophobic-Region-Induced Transitions in Self-Assembled Peptide Nanostructures. *Langmuir* **2009**, *25*, 4115–4123.
32. Yu, Y. C.; Pakalns, T.; Dori, Y.; McCarthy, J. B.; Tirrell, M.; Fields, G. B. Construction of Biologically Active Protein Molecular Architecture Using Self-Assembling Peptide-Amphiphiles. *Methods Enzymol.* **1997**, *289*, 571–587.
33. Gore, T.; Dori, Y.; Talmon, Y.; Tirrell, M.; Bianco-Peled, H. Self-Assembly of Model Collagen Peptide Amphiphiles. *Langmuir* **2001**, *17*, 5352–5360.
34. Vauthey, S.; Santoso, S.; Gong, H. Y.; Watson, N.; Zhang, S. G. Molecular Self-Assembly of Surfactant-Like Peptides to Form Nanotubes and Nanovesicles. *Proc. Natl. Acad. Sci. U.S.A.* **2002**, *99*, 5355–5360.
35. Bakota, E. L.; Sensoy, O.; Ozgur, B.; Sayar, M.; Hartgerink, J. D. Self-Assembling Multidomain Peptide Fibers with Aromatic Cores. *Biomacromolecules* **2013**, *14*, 1370–1378.
36. Dong, H.; Paramonov, S. E.; Aulisa, L.; Bakota, E. L.; Hartgerink, J. D. Self-Assembly of Multidomain Peptides: Balancing Molecular Frustration Controls Conformation and Nanostructure. *J. Am. Chem. Soc.* **2007**, *129*, 12468–12472.
37. Lakshmanan, A.; Hauser, C. A. E. Ultrasmall Peptides Self-Assemble into Diverse Nanostructures: Morphological Evaluation and Potential Implications. *Int. J. Mol. Sci.* **2011**, *12*, 5736–5746.
38. Nam, K. T.; Shelby, S. A.; Choi, P. H.; Marciel, A. B.; Chen, R.; Tan, L.; Chu, T. K.; Mesch, R. A.; Lee, B. C.; Connolly, M. D.; et al. Free-Floating Ultrathin Two-Dimensional Crystals from Sequence-Specific Peptoid Polymers. *Nature Mater.* **2010**, *9*, 454–460.
39. Sanii, B.; Kudirka, R.; Cho, A.; Venkateswaran, N.; Olivier, G. K.; Olson, A. M.; Tran, H.; Harada, R. M.; Tan, L.; Zuckermann, R. N. Shaken, Not Stirred: Collapsing a Peptoid Monolayer to Produce Free-Floating, Stable Nanosheets. *J. Am. Chem. Soc.* **2011**, *133*, 20808–20815.
40. Yue, K.; Dill, K. A. Forces of Tertiary Structural Organization in Globular Proteins. *Proc. Natl. Acad. Sci. U.S.A.* **1995**, *92*, 146–150.
41. Yue, K.; Dill, K. A. Inverse Protein Folding Problem: Designing Polymer Sequences. *Proc. Natl. Acad. Sci. U.S.A.* **1992**, *89*, 4163–4167.
42. Agashe, V. R.; Shastry, M. C.; Udgaonkar, J. B. Initial Hydrophobic Collapse in the Folding of Barstar. *Nature* **1995**, *377*, 754–757.
43. Sosnick, T. R.; Mayne, L.; Englander, S. W. Molecular Collapse: The Rate-Limiting Step in Two-State Cytochrome C Folding. *Proteins* **1996**, *24*, 413–426.
44. Bella, J.; Eaton, M.; Brodsky, B.; Berman, H. M. Crystal and Molecular Structure of a Collagen-Like Peptide at 1.9 Å Resolution. *Science* **1994**, *266*, 75–81.
45. Hulmes, D. J.; Miller, A.; Parry, D. A.; Piez, K. A.; Woodhead-Galloway, J. Analysis of the Primary Structure of Collagen for the Origins of Molecular Packing. *J. Mol. Biol.* **1973**, *79*, 137–148.
46. Hulmes, D. J.; Miller, A.; Parry, D. A.; Woodhead-Galloway, J. Fundamental Periodicities in the Amino Acid Sequence of the Collagen Alpha1 Chain. *Biochem. Biophys. Res. Commun.* **1977**, *77*, 574–580.
47. Kar, K.; Ibrar, S.; Nanda, V.; Getz, T. M.; Kunapuli, S. P.; Brodsky, B. Aromatic Interactions Promote Self-Association of Collagen Triple-Helical Peptides to Higher-Order Structures. *Biochemistry* **2009**, *48*, 7959–7968.
48. Jiang, T.; Xu, C.; Liu, Y.; Liu, Z.; Wall, J. S.; Zuo, X.; Lian, T.; Salaita, K.; Ni, C.; Pochan, D.; et al. Structurally Defined Nanoscale Sheets from Self-Assembly of Collagen-Mimetic Peptides. *J. Am. Chem. Soc.* **2014**, *136*, 4300–4308.
49. Jiang, T.; Xu, C.; Zuo, X.; Conticello, V. P. Structurally Homogeneous Nanosheets from Self-Assembly of a Collagen-Mimetic Peptide. *Angew. Chem., Int. Ed.* **2014**, *53*, 8367–8371.
50. Rele, S.; Song, Y.; Apkarian, R. P.; Qu, Z.; Conticello, V. P.; Chaikof, E. L. D-Periodic Collagen-Mimetic Microfibers. *J. Am. Chem. Soc.* **2007**, *129*, 14780–14787.

51. O'Leary, L. E.; Fallas, J. A.; Bakota, E. L.; Kang, M. K.; Hartgerink, J. D. Multi-Hierarchical Self-Assembly of a Collagen Mimetic Peptide from Triple Helix to Nanofibre and Hydrogel. *Nature Chem.* **2011**, *3*, 821–828.
52. Pires, M. M.; Chmielewski, J. Self-Assembly of Collagen Peptides into Microfibrillar Networks via Metal Coordination. *J. Am. Chem. Soc.* **2009**, *131*, 2706–2712.
53. Pires, M. M.; Lee, J.; Ernenwein, D.; Chmielewski, J. Controlling the Morphology of Metal-Promoted Higher Ordered Assemblies of Collagen Peptides with Varied Core Lengths. *Langmuir* **2012**, *28*, 1993–1997.
54. Przybyla, D. E.; Chmielewski, J. Metal-Triggered Collagen Peptide Disk Formation. *J. Am. Chem. Soc.* **2010**, *132*, 7866–7867.
55. Przybyla, D. E.; Chmielewski, J. Metal-Triggered Radial Self-Assembly of Collagen Peptide Fibers. *J. Am. Chem. Soc.* **2008**, *130*, 12610–12611.
56. Przybyla, D. E.; Rubert Perez, C. M.; Gleaton, J.; Nandwana, V.; Chmielewski, J. Hierarchical Assembly of Collagen Peptide Triple Helices into Curved Disks and Metal Ion-Promoted Hollow Spheres. *J. Am. Chem. Soc.* **2013**, *135*, 3418–3422.
57. Xu, F.; Li, J.; Jain, V.; Tu, R. S.; Huang, Q.; Nanda, V. Compositional Control of Higher Order Assembly Using Synthetic Collagen Peptides. *J. Am. Chem. Soc.* **2012**, *134*, 47–50.
58. Kotch, F. W.; Raines, R. T. Self-Assembly of Synthetic Collagen Triple Helices. *Proc. Natl. Acad. Sci. U.S.A.* **2006**, *103*, 3028–3033.
59. Cejas, M. A.; Kinney, W. A.; Chen, C.; Vinter, J. G.; Almond, H. R., Jr.; Balss, K. M.; Maryanoff, C. A.; Schmidt, U.; Breslav, M.; Mahan, A.; et al. Thrombogenic Collagen-Mimetic Peptides: Self-Assembly of Triple Helix-Based Fibrils Driven by Hydrophobic Interactions. *Proc. Natl. Acad. Sci. U.S.A.* **2008**, *105*, 8513–8518.
60. Witten, T. A.; Sander, L. M. Diffusion-Limited Aggregation. *Phys. Rev. B* **1983**, *27*, 5686–5697.
61. Witten, T. A.; Sander, L. M. Diffusion-Limited Aggregation, a Kinetic Critical Phenomenon. *Phys. Rev. Lett.* **1981**, *47*, 1400–1403.
62. Mu, Y.; Yu, M. Effects of Hydrophobic Interaction Strength on the Self-Assembled Structures of Model Peptides. *Soft Matter* **2014**, *10*, 4956–4965.
63. Narayanan, B.; Gilmer, G. H.; Tao, J.; De Yoreo, J. J.; Ciobanu, C. C. Self-Assembly of Collagen on Flat Surfaces: The Interplay of Collagen–Collagen and Collagen–Substrate Interactions. *Langmuir* **2014**, *30*, 1343–1350.
64. Lovelady, H. H.; Shashidhara, S.; Matthews, W. G. Solvent Specific Persistence Length of Molecular Type I Collagen. *Biopolymers* **2014**, *101*, 329–335.
65. Lomander, A.; Hwang, W.; Zhang, S. Hierarchical Self-Assembly of a Coiled-Coil Peptide into Fractal Structure. *Nano Lett.* **2005**, *5*, 1255–1260.
66. Han, T. H.; Oh, J. K.; Lee, G. J.; Pyun, S. I.; Kim, S. O. Hierarchical Assembly of Diphenylalanine into Dendritic Nanoarchitectures. *Colloids Surf. B Biointerfaces* **2010**, *79*, 440–445.
67. Song, H.; Parkinson, J. Modelling the Self-Assembly of Elastomeric Proteins Provides Insights into the Evolution of Their Domain Architectures. *PLoS Comput. Biol.* **2012**, *8*, e1002406.
68. Parkinson, J.; Kadler, K. E.; Brass, A. Simple Physical Model of Collagen Fibrillogenesis Based on Diffusion Limited Aggregation. *J. Mol. Biol.* **1995**, *247*, 823–831.
69. Kadler, K. E.; Hojima, Y.; Prockop, D. J. Collagen Fibrils *in vitro* Grow from Pointed Tips in the C- to N-Terminal Direction. *Biochem. J.* **1990**, *268*, 339–343.
70. Prockop, D. J.; Fertala, A. The Collagen Fibril: The Almost Crystalline Structure. *J. Struct. Biol.* **1998**, *122*, 111–118.
71. Persikov, A. V.; Ramshaw, J. A.; Brodsky, B. Prediction of Collagen Stability from Amino Acid Sequence. *J. Biol. Chem.* **2005**, *280*, 19343–19349.
72. Kar, K.; Wang, Y. H.; Brodsky, B. Sequence Dependence of Kinetics and Morphology of Collagen Model Peptide Self-Assembly into Higher Order Structures. *Protein Sci.* **2008**, *17*, 1086–1095.
73. Xu, F.; Khan, I. J.; McGuinness, K.; Parmar, A. S.; Silva, T.; Murthy, N. S.; Nanda, V. Self-Assembly of Left- and Right-Handed Molecular Screws. *J. Am. Chem. Soc.* **2013**, *135*, 18762–18765.
74. Brodsky, B.; Eikenberry, E. F. Characterization of Fibrous Forms of Collagen. *Methods Enzymol.* **1982**, *82* (Part A), 127–174.
75. Garbuzyanskiy, S. O.; Lobanov, M. Y.; Galzitskaya, O. V. Foldamlyloid: A Method of Prediction of Amyloidogenic Regions from Protein Sequence. *Bioinformatics* **2010**, *26*, 326–332.
76. Hwang, E. S.; Thiagarajan, G.; Parmar, A. S.; Brodsky, B. Interruptions in the Collagen Repeating Tripeptide Pattern Can Promote Supramolecular Association. *Protein Sci.* **2010**, *19*, 1053–1064.
77. Klunk, W. E.; Jacob, R. F.; Mason, R. P. Quantifying Amyloid by Congo Red Spectral Shift Assay. *Methods Enzymol.* **1999**, *309*, 285–305.
78. Aggeli, A.; Nyrkova, I. A.; Bell, M.; Harding, R.; Carrick, L.; McLeish, T. C.; Semenov, A. N.; Boden, N. Hierarchical Self-Assembly of Chiral Rod-Like Molecules as a Model for Peptide Beta-Sheet Tapes, Ribbons, Fibrils, and Fibers. *Proc. Natl. Acad. Sci. U.S.A.* **2001**, *98*, 11857–11862.
79. Matson, J. B.; Newcomb, C. J.; Bitton, R.; Stupp, S. I. Nanostructure-Templated Control of Drug Release from Peptide Amphiphile Nanofiber Gels. *Soft Matter* **2012**, *8*, 3586–3595.
80. Webber, M. J.; Berns, E. J.; Stupp, S. I. Supramolecular Nanofibers of Peptide Amphiphiles for Medicine. *Isr. J. Chem.* **2013**, *53*, 530–554.
81. Burkoth, T. S.; Beausoleil, E.; Kaur, S.; Tang, D.; Cohen, F. E.; Zuckermann, R. N. Toward the Synthesis of Artificial Proteins: The Discovery of an Amphiphilic Helical Peptoid Assembly. *Chem. Biol.* **2002**, *9*, 647–654.
82. Niesen, F. H.; Berglund, H.; Vedadi, M. The Use of Differential Scanning Fluorimetry to Detect Ligand Interactions That Promote Protein Stability. *Nat. Protoc.* **2007**, *2*, 2212–2221.
83. Emsley, J.; Knight, C. G.; Farndale, R. W.; Barnes, M. J.; Liddington, R. C. Structural Basis of Collagen Recognition by Integrin Alpha2beta1. *Cell* **2000**, *101*, 47–56.
84. Haines-Butterick, L.; Rajagopal, K.; Branco, M.; Salick, D.; Rughani, R.; Pilarz, M.; Lamm, M. S.; Pochan, D. J.; Schneider, J. P. Controlling Hydrogelation Kinetics by Peptide Design for Three-Dimensional Encapsulation and Injectable Delivery of Cells. *Proc. Natl. Acad. Sci. U.S.A.* **2007**, *104*, 7791–7796.
85. Faruqui, N.; Bella, A.; Ravi, J.; Ray, S.; Lamarre, B.; Ryadnov, M. G. Differentially Instructive Extracellular Protein Micro-Nets. *J. Am. Chem. Soc.* **2014**, *136*, 7889–7898.
86. Savitzky, A.; Golay, M. J. E. Smoothing and Differentiation of Data by Simplified Least Squares Procedures. *Anal. Chem.* **1964**, *36*, 1627–1639.
87. Nečas, D.; Klapetek, P. Gwyddion: An Open-Source Software for SPM Data Analysis. *Centr. Eur. J. Phys.* **2012**, *10*, 181–188.
88. Horcas, I.; Fernandez, R.; Gomez-Rodriguez, J. M.; Colchero, J.; Gomez-Herrero, J.; Baro, A. M. Wsxrm: A Software for Scanning Probe Microscopy and a Tool for Nanotechnology. *Rev. Sci. Instrum.* **2007**, *78*, 013705.
89. MATLAB, Version 8.0.3.0 (R2014a); The MathWorks, Inc.: Natick, MA, 2014.